MATERIALS CHEMISTRY FRONTIERS

CHINESE CHEMICAL SOCIETY

ROYAL SOCIETY OF CHEMISTRY

RESEARCH ARTICLE

View Article Online
View Journal | View Issue

Cite this: *Mater. Chem. Front.*, 2023, **7**, 2454

Red-shift emission and rapid up-conversion of B,N-containing electroluminescent materials *via* tuning intramolecular charge transfer†

Yi-Hui He,[a] Feng-Ming Xie,*[a] Hao-Ze Li,[b] Kai Zhang,[c] Yang Shen,[a] Feng Ding,[a] Cheng-Yuan Wang,[a] Yan-Qing Li*[b] and Jian-Xin Tang *[ac]

Received 12th February 2023,
Accepted 20th March 2023

DOI: 10.1039/d3qm00131h

rsc.li/frontiers-materials

Boron (B) and nitrogen (N)-based polycyclic aromatic hydrocarbons (PAHs) have been demonstrated as promising materials for building efficient thermally activated delayed fluorescent (TADF) emitters in blue and green regions, while red emission materials based on B,N systems are rare. Hence, to achieve a red-shifted emission peak over 600 nm by simply modifying the core of B,N-PAHs is a rewarding and challenging task. In this work, we demonstrate the *para*-D–π–B strategy implementation of modulating the predominance of locally excited (LE)/charger transfer (CT) states by introducing peripheral electron-donating units in a boron-carbazole containing backbone (**BNCz**) to develop four TADF emitters, **BN-TC**, **BN-AC**, **BN-PXZ** and **BN-PZ**. Due to the effect of different donor strengths on the excited states of these materials, we obtain full-color emission and a high photoluminescence quantum yield (Φ_{PL}) of nearly 100%. Notably, the device employing **BN-PZ** as a dopant exhibits orange-red emission with an electroluminescence (EL) peak at 612 nm. Meanwhile, this compound realizes very fast reverse intersystem crossing (RISC) with a rate constant (k_{RISC}) of 1.8 × 10^6 s^{-1}, resulting in a device with a high external quantum efficiency (EQE) of 25.0% and low efficiency roll-off at high brightness.

1. Introduction

Organic light-emitting diodes (OLEDs) are now the star product in the full-color display and solid-state lighting fields. The internal quantum efficiency (IQE) of OLEDs based on pure organic TADF emitters is up to 100%, as 75% of the triplet excitons can be transferred from the lowest triplet (T_1) excited state to the lowest singlet (S_1) excited state by the reverse intersystem crossing process.[1–3] In order to achieve an efficient RISC process, a small singlet–triplet splitting energy (ΔE_{ST}) between S_1 and T_1 in TADF materials is the critical point, which requires the overlap between the highest occupied molecular orbitals (HOMO) and the lowest unoccupied molecular orbitals (LUMO) to be as small as possible.[4–9] The most widespread TADF molecular design strategy is the use of highly distorted donor–acceptor (D–A) structures.[10–13] The twisted D–A framework accompanied by the intramolecular charge transfer (ICT) characteristic allows TADF materials to easily exhibit full-color emission, which is essential for color displays, white lighting, imaging applications, *etc.*[14–16]

In 2016, Hatakeyama and co-workers developed novel PAHs containing boron (B) and nitrogen (N) atoms. This B,N-based TADF material features outstanding blue emission with a high Φ_{PL} and small ΔE_{ST}.[17] B,N-based TADF materials emitting in blue and green regions are currently booming, owing to great efforts that have been made to modify and innovate this B,N-based core through different strategies. Duan *et al.* and Wang *et al.* both introduced acceptors at the *para*-carbon position of B-substituted phenyl rings (*para*-A–π–B), which could modulate the LUMO distribution and excited state of the molecule to red-shift the emission wavelength, resulting in efficient green OLEDs.[18,19] Chou and co-workers reported a series of B,N-based TADF materials with green emission *via* the design approach of introducing sulfur atoms into the B,N-based core.[20,21] Yasuda's group and Yang's group obtained highly-efficient yellow devices by a peripheral decoration strategy on the B,N-based core (*para*-D–π–N and *peri*-D–π–N).[22,23] Recently, Duan and co-workers reported deep-red B,N-based TADF materials *via* the design approach of the *para*-B–π–B method.[24] Regrettably, on the one hand, B,N-based TADF emitters in longer wavelength regions with emission peaks

[a] *Jiangsu Key Laboratory for Carbon-Based Functional Materials & Devices, Institute of Functional Nano & Soft Materials (FUNSOM), Soochow University, Suzhou, Jiangsu 215123, China. E-mail: fmxie@suda.edu.cn, jxtang@suda.edu.cn*
[b] *School of Physics and Electronic Science, East China Normal University, Shanghai 200062, China. E-mail: yqli@phy.ecnu.edu.cn*
[c] *Macao Institute of Materials Science and Engineering (MIMSE), Faculty of Innovation Engineering, Macau University of Science and Technology, Taipa, Macao 999078, China*

† Electronic supplementary information (ESI) available. See DOI: https://doi.org/10.1039/d3qm00131h

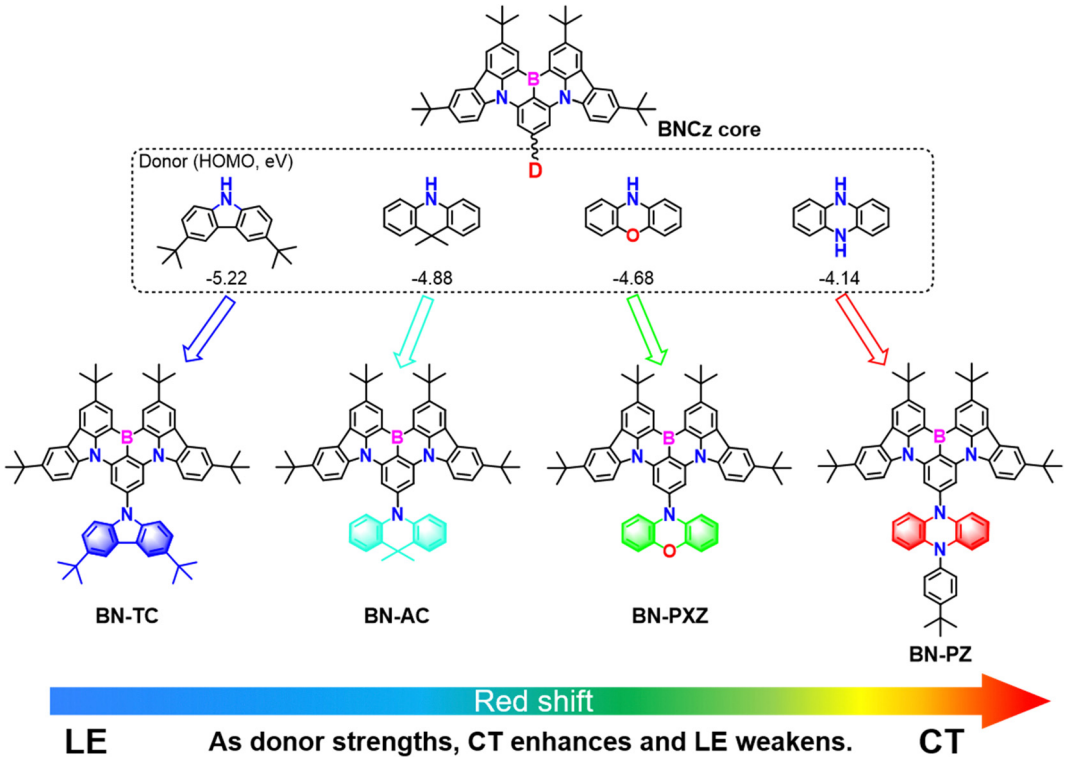

Fig. 1 Design for full-color TADF emitters based on boron–nitrogen embedded polycyclic aromatic hydrocarbon as well as chemical structures of **BNCz**, **BN-TC**, **BN-AC**, **BN-PXZ** and **BN-PZ**.

exceeding 600 nm remain scarce, while on the other hand, the up-conversion rates of these TADF materials are still limited to a magnitude order of 10^4 s^{-1}, leading to severe triplet–triplet annihilation (TTA) and triplet–polaron annihilation (TPA). Hence, developing new schemes for obtaining red-shifting B,N-containing PAHs with high up-conversion rates is in urgent demand for producing efficient and low roll-off red TADF-OLEDs.

Herein, we propose and practice a novel strategy of modulating the HOMO level and predominance of locally excited (LE)/charger transfer (CT) states by introducing a donor. In detail, we introduce donors with different HOMO energy levels at the *para*-position of the B atom in the **BNCz** core,[25,26] as shown in Fig. 1, namely, **BN-TC**, **BN-AC**, **BN-PXZ** and **BN-PZ**. It is worth noting that **BNCz** is not only an MR-TADF molecule,[18,27,28] but it can also act as an acceptor in the D–A skeleton. When increasing the interaction strength of the donors, the excited state properties gradually tend from LE towards CT. As a result, we have succeeded in achieving full-color emissions from 464 nm to 634 nm in toluene through donor engineering. These TADF emitters exhibit high Φ_{PL}s of nearly 100% and a remarkably elevated RISC rate (10^6 s^{-1}) is obtained for **BN-PZ**. The corresponding blue and green devices achieve maximum external quantum efficiencies (EQE) of over 20%. Notably, the **BN-PZ**-based OLEDs display orange-red emission peaking at 612 nm, and a high maximum EQE of 25.0% with significantly low efficiency roll-off. A remarkable EQE of 17.6% at 1000 cd m^{-2} is the highest value reported for sensitizer-free TADF OLEDs with EL peaks over 610 nm so far. This work confirms that modulating the predominance of the LE/CT state is an effective method to realize red-shifted emission in B–N-containing PAHs.

2. Results and discussion

2.1. Molecular design and synthesis

Three designed boron-carbazole containing emitters, namely, **BN-AC**, **BN-PXZ** and **BN-PZ**, were synthesized by a nucleophilic aromatic substitution reaction and tandem electrophilic arene borylation (Experimental Section and Scheme S1 in the ESI†). These emitters have been characterized by ^{1}H NMR, ^{13}C NMR, and time of flight mass spectrometry (Fig. S1–S9, ESI†). All final products were purified by temperature-gradient sublimation under vacuum after recrystallization and the purity requirements of fabrication for OLEDs were achieved by vacuum deposition. Thermogravimetric analysis (TGA) and differential scanning calorimetry (DSC) indicated the excellent thermal stabilities of **BN-AC**, **BN-PXZ** and **BN-PZ**, with 5% weight-loss decomposition temperatures (T_d) of 440 °C, 453 °C and 454 °C, respectively, and glass transition signals (T_g) of 253 °C, 268 °C and 271 °C, respectively (Fig. S10, ESI†). Such excellent thermal stability of these emitters is consistent with their rigid configurations, which fulfills the requirement of thermal evaporation. The single crystal structure of **BN-PZBN-PZ** was obtained from a toluene/CH_2Cl_2 mixed solution, as shown in Fig. S11 and S12 (ESI†) (CCDC number: 2241686†), revealing a highly distorted molecular geometry with a large dihedral angle of 84.9° between

the B,N-core and phenazine. The twisted D–A structure and the strongest PZ donor could strengthen the ICT state, enabling the simultaneous realization of long-wavelength emission.

2.2. Theoretical calculations

To understand the effect of different *para*-donor units of the backbone on molecular geometry and optoelectronic properties, density functional theory (DFT) and time-dependent DFT (TD-DFT) calculations were performed using the B3LYP functional with the 6-31G(d) basis set in the Gaussian 16 program. The frontier orbital distributions and energy levels of these compounds are depicted in Fig. 2. The dihedral angles of the twisted D–A structure are estimated to be 52°, 84°, 74° and 77° for **BN-TC**, **BN-AC**, **BN-PXZ** and **BN-PZ**, respectively. The large dihedral angles are beneficial for enhancing the ICT character and lowering ΔE_{ST}. **BN-TC** shows a delocalized HOMO–LUMO distribution, whereas the HOMO and LUMO orbitals of **BN-AC**, **BN-PXZ** and **BN-PZ** are separated. In addition, the energy gap (E_g), S_1 and T_1 all decrease as the donor strength increases, which could cause spectral red-shifts. They also exhibit large oscillator strengths (f)of 0.3912, 0.4139, 0.4163 and 0.3444, indicating a fast-radiative decay and high Φ_{PL}.

Furthermore, the natural transition orbitals (NTOs) of S_1 and triplet (T_n) excited states of these materials were calculated and are shown in Fig. 3. The S_1 excited states of all three molecules show completely separated "holes" and "particles" respectively located on the donor and **BNCz** core, but their T_n excited states are distinguishing. For **BN-AC**, the ΔE_{ST} between the S_1 and T_1 excited state is 0.110 eV, while ΔE_{ST} between the S_1 and second triplet (T_2) excited state is 0.010 eV, which seems small enough to establish a feasible RISC channel. However, the S_1 and T_2 excited states have highly similar CT features, which forbids spin–orbital coupling (SOC) between them, and therefore invalidates $T_2 \rightarrow S_1$ RISC.[28] In addition, the simulated SOC matrix element ($\langle S|\hat{H}_{SOC}|T\rangle$) between the LE-predominant T_1 excited state and S_1 excited state of **BN-AC** reaches 0.436 cm^{-1} ($\langle S_1|\hat{H}_{SOC}|T_1\rangle = 0.436\,cm^{-1}$), which is one order of magnitude higher than that between T_2 and S_1 ($\langle S_1|\hat{H}_{SOC}|T_2\rangle = 0.0283\,cm^{-1}$). The T_2 excited state of **BN-PXZ** is mainly centralized on the **BNCz** core, corresponding to LE-predominance. Despite a smaller energy gap between its T_1 and S_1, T_1 can also not support RISC to S_1, because its CT feature induced vanishing of SOC. Meanwhile, SOC of the $S_1 \rightarrow T_1$ excitation sharply decreases by several times, compared to that of $S_1 \rightarrow T_2$ excitation ($\langle S_1|\hat{H}_{SOC}|T_1\rangle = 0.071\,cm^{-1}$, $\langle S_1|\hat{H}_{SOC}|T_2\rangle = 0.312\,cm^{-1}$). The T_1 excited state of **BN-PZ** exhibits a similar "hole" and "particle" distribution to S_1, while T_2 is unable to establish a transition channel with S_1, due to an unbridgeable energy gap. In a word, both **BN-AC** and **BN-PXZ** simultaneously contain CT-predominant S_1 and LE-predominant T_n excited states, while **BN-PZ** only has the CT feature, demonstrating that excited states convert from LE-predominant to CT-predominant with increasing donor strength, in which a limit that determines the role of the BN core as an emitter or an acceptor probably exists. More specifically, on connecting a *para*-donor with a shallower HOMO energy level than that of PXZ, the molecule will exhibit a CT-predominant excited state, while the **BNCz** core will act as an

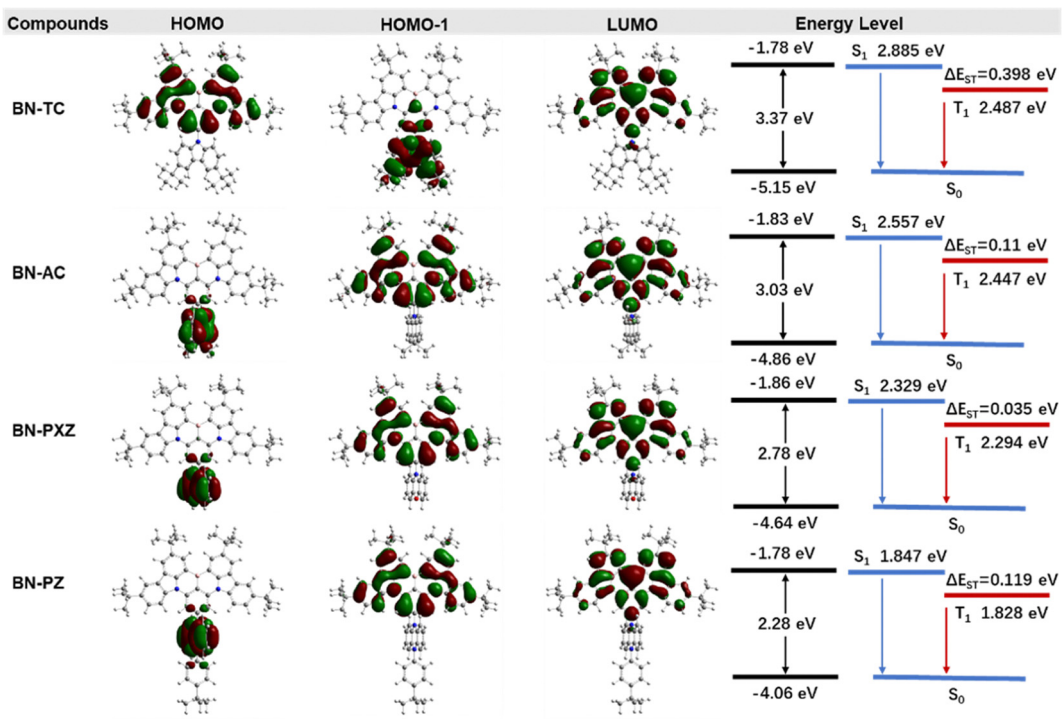

Fig. 2 Distributions of frontier molecular orbitals, calculated energy gaps and energy-level diagrams for the singlet and triplet excited states of **BN-TC**, **BN-AC**, **BN-PXZ** and **BN-PZ**.

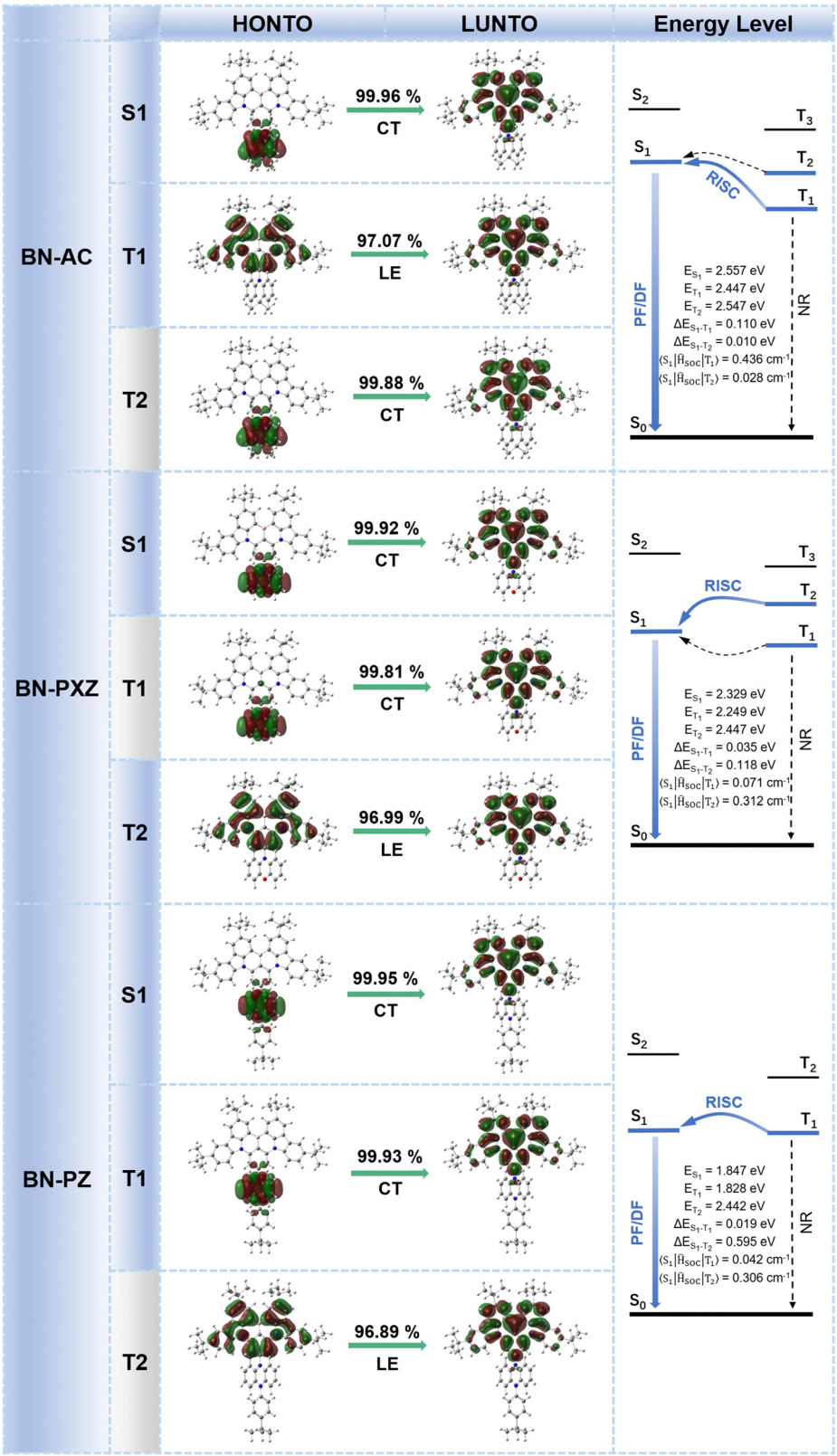

Fig. 3 Energy-level diagrams and related NTOs for the singlet and triplet excited states of **BN-AC**, **BN-PXZ** and **BN-PZ**. Transition energies for S_1 and T_n (n = 1, 2) and the SOC matrix elements were calculated at the B3LYP/6-31G(d) levels of theory, respectively.

acceptor. In this case, we predict that **BN-AC** and **BN-PXZ** should exhibit narrow-band emissions combined with the CT feature, while **BN-PZ** is identical to common D–A type molecules with broad emission.

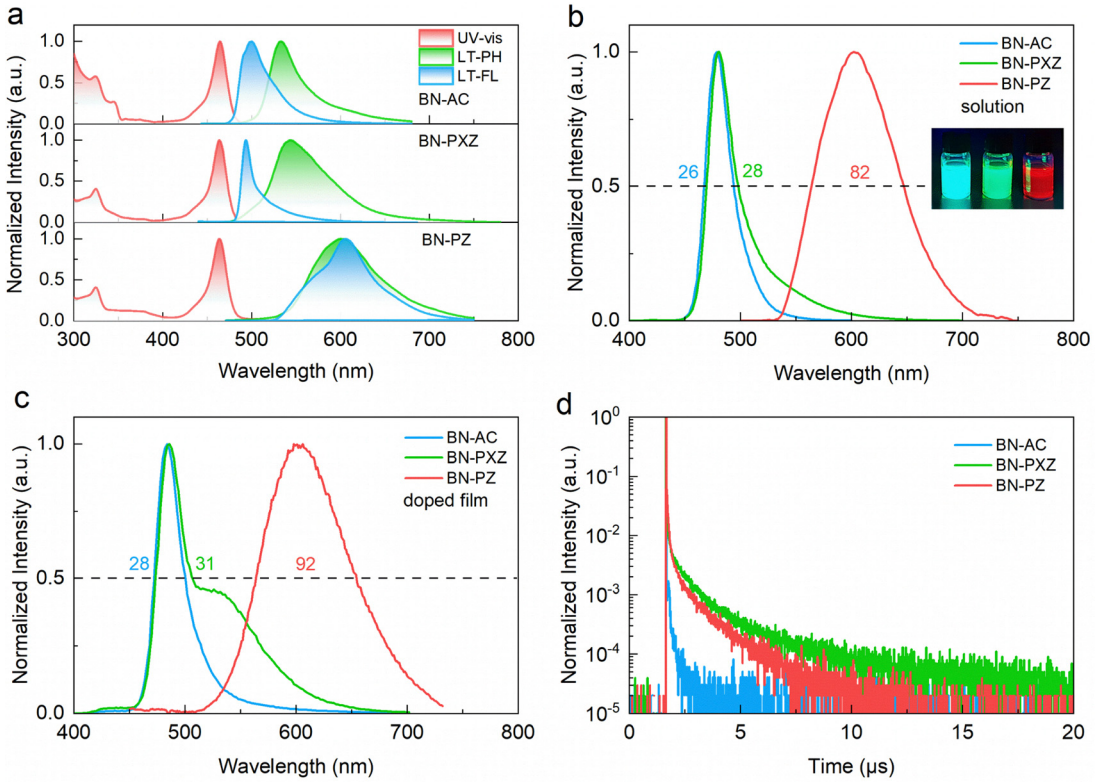

Fig. 4 (a) UV-vis absorption (Abs., in 1×10^{-5} M toluene), steady-state fluorescence (LT-FL, 77 K in neat films), and phosphorescence (LT-Ph, 77 K in neat films) spectra. (b) Photoluminescence spectra in toluene (1×10^{-5} M). (c) Photoluminescence spectra in 15 wt% doped films (host: mCBP). (d) Transient photoluminescence decay profiles (doped films *in vacuo*).

2.3. Photophysical properties

The photophysical spectroscopic properties of **BN-AC**, **BN-PXZ** and **BN-PZ** are shown in Fig. 4, and the key data are summarized in Table 1. As predicted by DFT calculations, the UV absorption of these materials shows a strong MR characteristic peak at ~464 nm, which originates from the B,N-containing framework. Due to the shallowest HOMO energy level of the donor PZ, **BN-PZ** has an additional low energy ICT absorption band at 490–550 nm (Fig. S13, ESI†) and exhibits red emission with a peak at 634 nm in a dilute toluene solution (Fig. 4b). The S_1 and T_1 energy values are obtained from the onset wavelength of low-temperature fluorescence and phosphorescence spectra, based on which the ΔE_{ST} values are calculated to be 0.14 eV, 0.12 eV and 0.03 eV for **BN-AC**, **BN-PXZ** and **BN-PZ**, respectively. Such a tiny ΔE_{ST} can benefit efficient recycling of the triplet excitons *via* the rapid RISC process. The PL spectra of **BN-AC** and **BN-PXZ** in dilute toluene are almost identical, resulting from the similar emissions in solution originating from their LE states, but the curve of **BN-PXZ** in the region over 510 nm is relatively higher than that of **BN-AC**, which is consistent with the stronger CT state of **BN-PXZ** (Fig. 4b). The solvent polarity-dependent emission behaviors of emitters were studied using the Lippert–Mataga model, in which the *X*-axis stands for the solvent polarity factor *f*, and the *Y*-axis represents Stokes' shift (Fig. S14 and Table S2, ESI†). The UV-vis absorption spectrum of **BN-AC** and **BN-PXZ** showed a slight change within a scope of 5 nm as the solvent polarity increased, indicating a negligible dipolar change in the S_0 state with the change in solvent polarity. The dipole moment of S_1 excitons can be estimated from the fitted line of experimental points. Their two-section lines corresponded to the two different exciton states with two distinguishable small and large dipole moments in low-polarity

Table 1 Physical properties of **BNCz**, **BN-TC**, **BN-AC**, **BN-PXZ** and **BN-PZ**

Compounds	λ_{abs}[a] (nm)	λ_{em}[a] (nm)	FWHM[a] (nm)	Stokes shift[a] (nm)	$E_{S1}/E_{T1}/\Delta E_{ST}$[c] (eV)	HOMO/LUMO[d] (eV)	T_d[e] (°C)
BNCz[f]	467	481	44	14	2.66/2.53/0.13	−5.40/−2.85	—
BN-TC	460	464	22	4	2.64/2.50/0.14	−5.46/−2.85	—
BN-AC	464	479 (484)[b]	26	14	2.59/2.45/0.14	−5.33/−2.74	447
BN-PXZ	464	480 (486)[b]	28	14	2.57/2.45/0.12	−5.14/−2.55	458
BN-PZ	464	634 (610)[b]	82	70	2.34/2.31/0.03	−4.58/−1.99	466

[a] In toluene, 1.0×10^{-5} M. [b] λ_{em} measured in the 15%-doped film in mCBP host. [c] E_{S1} and E_{T1} were determined from the onsets of LTFL and LTPh, respectively; $\Delta E_{ST} = E_{S1} - E_{T1}$. [d] HOMO levels were determined from the onset of the oxidation curves, and LUMO levels were calculated by using the HOMO levels and E_g. [e] Measured from thermal gravimetric analysis (TGA). [f] Literature.[19,28,29]

and high-polarity solvents, respectively. In the case of low-polarity solvents, the S_1 excitons of **BN-AC** and **BN-PXZ** behaved as LE states with small dipole moments of 4.47 D and 7.54 D, respectively, while their S_1 excitons exhibited large dipole moments of 14.23 D and 14.02 D, respectively, in high-polarity solvents, which clearly illustrated a considerable contribution of ICT character in the excited state. Compared with the other emitters, **BN-PZ** exhibits only CT-dominant emission in both low- and high-polarity solvents, demonstrating the ICT characteristic expected from molecular design. In addition, **BN-PZ** exhibits a wider photoluminescence (PL) spectrum than the others, resulting from dominance of the CT state rather than the LE state, which is consistent with the theory of spontaneous emission that the full width at half maximum (FWHM) is proportional to the square of the emission peak wavelength.[29] When doped in a 3,3′-bis(carbazol-9-yl)biphenyl (mCBP) host, all three materials display slightly broadened spectra due to π–π interactions (Fig. 4c). It is noted that, due to the host–guest interaction, the CT state also participates in the emission in the doped film, in which **BN-PXZ** exhibits a red-shifted shoulder peak in the region over 510 nm. Moreover, the Φ_{PL} values in mCBP doped films are measured to be 94%, 97% and 98% for **BN-AC**, **BN-PXZ** and BN-PZ, exhibiting PL emission at 484 nm, 486 nm and 610 nm, respectively.

To further investigate the photophysical properties of these emitters, the transient PL spectra of the doped films in mCBP host matrix were recorded. As depicted in Fig. 4d, **BN-AC**, **BN-PXZ** and **BN-PZ** exhibited a significantly delayed fluorescence behavior owing to the small ΔE_{ST} values, showing prompt fluorescence lifetimes (τ_p)/delayed fluorescence lifetimes (τ_d) of 3.8 ns/9.7 μs, 8.9 ns/1.7 μs and 39.4 ns/1.2 μs, respectively. Thereinto, the **BN-AC**-based doped film displayed shorter τ_p compared to the tens of nanoseconds for **BN-PZ**, which is consistent with the gradual decreasing proportion of the prompt fluorescence component from **BN-AC** to **BN-PZ** (Table S3, ESI†). Moreover, the short τ_d value of about 1 μs of the **BN-PZ** is conducive to the rapid RISC process. Furthermore, by incorporating the large rate constants of singlet radiative decay, the concentration quenching of triplet excitons and efficiency roll-off in electroluminescent devices can be effectively alleviated at high brightness.[27,30] The temperature dependence of transient decay in the doped films clearly shows that the delayed fluorescence (DF) component increased progressively alone with rising temperature, indicating the TADF process in the molecules (Fig. S15, ESI†).

To understand the S_1 and T_1 exciton dynamic processes of these TADF emitters in doped films, the rate constants, such as singlet radiative decay rate constants (k_r), nonradiative decay rate constants (k_{nr}), internal conversion rate constants (k_{IC}), intersystem crossing rate constants (k_{ISC}), and reverse intersystem crossing rate constants (k_{RISC}) are estimated according to the formulas provided in the literature and summarized in the Table S3 (ESI†).[31–33] Resulting from the highly rigid planar parent core **BNCz** unit, the k_r values of these emitters are over 10^7 s^{-1}. Benefiting from the increasing ICT character and small ΔE_{ST}, the k_{RISC} value of **BN-PZ** is in the range of 10^6 s^{-1}, which is much higher than those of most of the reported **BNCz**-based

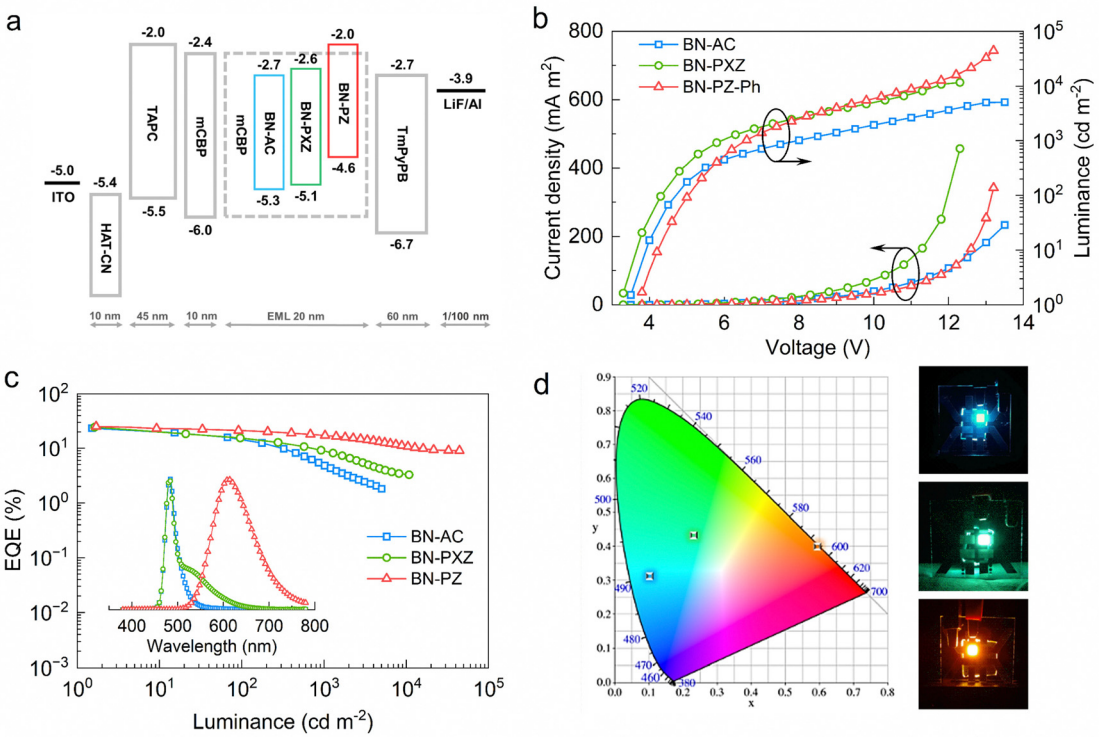

Fig. 5 (a) Device structure and energy level diagram of the materials used. (b) Current density and luminance *versus* voltage (*J*–*V*–*L*). (c) External quantum efficiency *versus* luminance (EQE-L) curves of the devices (inset: EL spectra of the devices). (d) The color coordinates of the devices on the CIE 1931 color space and the photographs showing the emission color of the 15 wt%-doping devices.

Table 2 The device performances of **BNCz**, **BN-TC**, **BN-AC**, **BN-PXZ** and **BN-PZ**

Compounds	V_{ON}[a] (V)	λ_{EL}[b] (nm)	FWHM[c] (nm)	L_{max}[d] (cd m^{-2})	CE_{max}[e] (cd A^{-1})	PE_{max}[f] (lm W^{-1})	EQE[g] (%)	CIE[h] (x, y)
BNCz	3.8	490	32	5017	34.3	29.0	21.1/13.0/5.9	(0.13, 0.41)
BN-TC	4.1	474	37	4448	28.2	21.6	21.2/8.7/4.2	(0.13, 0.20)
BN-AC	3.5	484	27	5089	35.1	31.5	23.4/15.9/5.5	(0.10, 0.31)
BN-PXZ	3.3	482	25	11710	51.2	48.7	24.4/15.5/8.2	(0.23, 0.43)
BN-PZ	3.8	612	104	44210	34.9	29.2	25.0/21.2/17.6	(0.60, 0.40)

[a] Turn-on voltage at 1 cd m^{-2}. [b] EL maximum wavelength. [c] Full width at half maximum. [d] Maximum luminance. [e] Maximum current efficiency. [f] Maximum power efficiency. [g] Maximum external quantum efficiency and values at 100 and 1000 cd m^{-2}. [h] Value at 100 cd m^{-2}.

TADF emitters, which suggests an efficient $T_1 \rightarrow S_1$ exciton up-conversion and high utilization of excitons.

2.4. Electroluminescent device performance

The EL properties of these TADF emitters were further investigated with the device structures of indium tin oxide (ITO)/1,4,5,8,9,11-hexaazatriphenylenehexacarbonitrile (HATCN, 10 nm)/di-[4-(*N*,*N*-ditolyl-amino)-phenyl] cyclohexane (TAPC, 60 nm)/3,3′-di(carbazol-9-yl)biphenyl (mCBP, 10 nm)/mCBP:*x* wt% emitters (20 nm)/1,3,5-tri(*m*-pyrid-3-ylphenyl)benzene (TmPyPB, 45 nm)/LiF (1 nm)/Al (100 nm). Herein, ITO and Al were used as the anode and cathode, respectively; HATCN and LiF served as the hole- and electron-injecting layers, respectively; TAPC and TmPyPB played the role of hole- and electron-transporting layers, respectively; mCBP acted as an electron blocking layer (EBL) and the host to form an emitting layer (EML). The corresponding energy level diagrams of each layer are illustrated in Fig. 5a. For the emitting layer, the optimized dopant concentration is 5 wt% for both **BNCz** and **BN-TC**, and 15 wt% for the other three TADF emitters (Fig. S16, ESI†). The current density–voltage–luminance (*J*–*V*–*L*) characteristics of these devices are shown in Fig. 5b and the key data of the devices are summarized in Table 2. The OLEDs based on **BN-AC** and **BN-PXZ** display attractively narrow EL emissions, with emission peaks at 484 nm and 482 nm, FWHM values of 27 nm and 25 nm, high maximum EQE values of 23.4% and 24.4%, and CIE coordinates of (0.10, 0.31) and (0.23, 0.43), respectively (Fig. 5c and 5d). Expectedly, the presence of a shoulder peak in the EL spectrum of **BN-PXZ** catches our attention. One explanation attributes this type of shoulder peak to dimer emission;[18,31] however, there is no shoulder peak in the EL spectrum of **BN-AC** with a similar conformation and dihedral angle. Hence, we propose a more plausible explanation: both LE state emission and relatively weak CT state emission exist in the emission of **BN-PXZ**, so a shoulder peak appears. And this is consistent with the NTO simulation results and PL spectra. Besides, the EL spectra of **BN-AC**, **BN-PXZ** and **BN-PZ** are highly stable under different operating voltages without emission shifting, and the device performances of **BNCz** and **BN-TC** are essentially the same as those reported in the literature. (Fig. S17 and S18, ESI†).[26,27] More importantly, the **BN-PZ**-based OLEDs exhibit prominent EL performances with a high maximum luminance (L_{max}) of 44210 cd m^{-2} and orange-red emission with a peak at 612 nm, which is in agreement with the PL spectra in doped films. Without using TADF-sensitizing fluorescence (TSF) technology, this device achieves a maximum EQE (EQE_{max}) as high as 25.0%. Furthermore, the **BN-PZ**-based device displays significantly alleviated efficiency roll-off of 15.2% and 29.6% with EQE values of 21.2% and 17.6% in 100 and 1000 cd m^{-2} (Fig. 5c and Table 2), respectively. In comparison with most sensitizer-free TADF OLEDs in the emission region over 610 nm, the **BN-PZ**-based device exhibits state-of-the-art EQE in 1000 cd m^{-2} and a lower efficiency roll-off, which can be attributed to the suppressed TTA and TPA in EML at high brightness due to its higher k_{RISC} (Fig. S19 and Table S4, ESI†).[4,14,16,34–59] Although the orange-red device displays high EQE and low efficiency roll-off, we expect to find a suitable TADF sensitizer that will be employed to further improve device efficiency and stability.

3. Conclusions

In conclusion, we propose a novel strategy of introducing a shallow HOMO-energy donor unit at the *para*-carbon position in the core of B,N-PAHs, effectively enabling red-shifted emission. Benefiting from a novel strategy of modulating the HOMO level and predominance of the LE/CT state, these TADF materials exhibit full-color emission and Φ_{PL} values of nearly 100%. The OLEDs based on these dopants achieve high EQEs of over 20%. Owing to the strong ICT character and faster RISC ($k_{RISC} > 10^6$ s^{-1}), the orange-red device utilizing **BN-PZ** as an emitter shows a maximum EQE of 25% with an emission peak at 612 nm, and attains a high maximum L_{max} of 44210 cd m^{-2} and low efficiency roll-off with a remarkable EQE of 17.6% in 1000 cd m^{-2}, which is the highest value reported for sensitizer-free TADF OLEDs with EL peaks over 610 nm so far. This work has provided a facile and effective strategy to modulate the LE/CT state of B,N-containing PAHs for efficient and stable red TADF-OLEDs.

4. Experimental section

Synthesis

Detailed synthetic procedure and general analysis of the materials are described in the ESI.†

Device fabrication and measurements

Devices were fabricated at a vacuum level lower than 1×10^{-4} Pa for both organic and metal layers. ITO coated glasses with a sheet resistance of 15 Ω square^{-1} were used as the substrate and cleaned with ultra-purified water and organic solvents, and then irradiated in UV-ozone for 15 min. Organic materials were evaporated to ITO at a rate of about 1 Å s^{-1}, while LiF and Al were evaporated at rates of around 0.1 and 5 Å s^{-1},

respectively. The intersection of ITO and the metal electrodes gave a 10 mm^2 active device area.

Conflicts of interest

The authors declare that they have no known competing financial interests or personal relationships that could have appeared to influence the work reported in this paper.

Acknowledgements

The authors acknowledge the financial support from the National Key R&D Program of China (no. 2022YFE0206100), the Science and Technology Development Fund (FDCT), Macau SAR (no. 0008/2022/AMJ), the National Natural Science Foundation of China (no. 62274117, 62075061), the Jiangsu Provincial department of Science and Technology (no. BZ2022054), the Science and Technology Innovation Plan Of Shanghai Science and Technology Commission (no. 22520760600), the Bureau of Science and Technology of Suzhou Municipality (no. SYC2022144), and the Collaborative Innovation Center of Suzhou Nano Science & Technology.

References

1 H. Uoyama, K. Goushi, K. Shizu, H. Nomura and C. Adachi, Highly efficient organic light-emitting diodes from delayed fluorescence, *Nature*, 2012, **492**, 234–238.
2 Y. Tao, K. Yuan, T. Chen, P. Xu, H. Li, R. Chen, C. Zheng, L. Zhang and W. Huang, Thermally Activated Delayed Fluorescence Materials Towards the Breakthrough of Organoelectronics, *Adv. Mater.*, 2014, **26**, 7931–7958.
3 Z. Yang, Z. Mao, Z. Xie, Y. Zhang, S. Liu, J. Zhao, J. Xu, Z. Chi and M. P. Aldred, Recent advances in organic thermally activated delayed fluorescence materials, *Chem. Soc. Rev.*, 2017, **46**, 915–1016.
4 J.-X. Chen, W.-W. Tao, W.-C. Chen, Y.-F. Xiao, K. Wang, C. Cao, J. Yu, S. Li, F.-X. Geng, C. Adachi, C.-S. Lee and X.-H. Zhang, Red/Near-Infrared Thermally Activated Delayed Fluorescence OLEDs with Near 100% Internal Quantum Efficiency, *Angew. Chem., Int. Ed.*, 2019, **58**, 14660–14665.
5 Y.-Z. Shi, K. Wang, S.-L. Zhang, X.-C. Fan, Y. Tsuchiya, Y.-T. Lee, G.-L. Dai, J.-X. Chen, C.-J. Zheng, S.-Y. Xiong, X.-M. Ou, J. Yu, J.-S. Jie, C.-S. Lee, C. Adachi and X.-H. Zhang, Characterizing the Conformational Distribution in an Amorphous Film of an Organic Emitter and Its Application in a ''Self-Doping'' Organic Light-Emitting Diode, *Angew. Chem., Int. Ed.*, 2021, **60**, 25878–25883.
6 L. Zhou, H. Wang, Y.-Z. Shi, X.-C. Fan, J.-X. Chen, K. Wang, J. Yu and X.-H. Zhang, Controlling the conjugation extension inside acceptors for enhancing reverse intersystem crossing of red thermally activated delayed fluorescence emitters, *Chem. Eng. J.*, 2022, **440**, 135775.
7 M. Zhang, C.-J. Zheng, K. Wang, Y.-Z. Shi, D.-Q. Wang, X. Li, H. Lin, S.-L. Tao and X.-H. Zhang, Hydrogen-Bond-Assisted Exciplex Emitters Realizing Improved Efficiencies and Stabilities in Organic Light Emitting Diodes, *Adv. Funct. Mater.*, 2021, **31**, 2010100.
8 Z. Li, D. Yang, C. Han, B. Zhao, H. Wang, Y. Man, P. Ma, P. Chang, D. Ma and H. Xu, Optimizing Charge Transfer and Out-Coupling of A Quasi-Planar Deep-Red TADF Emitter: towards Rec.2020 Gamut and External Quantum Efficiency beyond 30%, *Angew. Chem., Int. Ed.*, 2021, **60**, 14846–14851.
9 C.-C. Yan, X.-D. Wang and L.-S. Liao, Thermally Activated Delayed Fluorescent Gain Materials: Harvesting Triplet Excitons for Lasing, *Adv. Sci.*, 2022, **9**, 2200525.
10 S.-Y. Yang, Z.-Q. Feng, Z. Fu, K. Zhang, S. Chen, Y.-J. Yu, B. Zou, K. Wang, L.-S. Liao and Z.-Q. Jiang, Highly Efficient Sky-Blue π-Stacked Thermally Activated Delayed Fluorescence Emitter with Multi-Stimulus Response Properties, *Angew. Chem., Int. Ed.*, 2022, **61**, e202206861.
11 X. Tang, L.-S. Cui, H.-C. Li, A. J. Gillett, F. Auras, Y.-K. Qu, C. Zhong, S. T. E. Jones, Z.-Q. Jiang, R. H. Friend and L.-S. Liao, Highly efficient luminescence from space-confined charge-transfer emitters, *Nat. Mater.*, 2020, **19**, 1332–1338.
12 Y. Liu, J. Yang, Z. Mao, X. Chen, Z. Yang, X. Ge, X. Peng, J. Zhao, S.-J. Su and Z. Chi, Asymmetric Thermally Activated Delayed Fluorescence Emitter for Highly Efficient Red/Near-Infrared Organic Light-Emitting Diodes, *ACS Appl. Mater. Interfaces*, 2022, **14**, 33606–33613.
13 H.-Y. Yang, H.-y Zhang, M. Zhang, X.-c Fan, H. Lin, S.-L. Tao, C.-J. Zheng and X.-H. Zhang, Multiplying the efficiency of red thermally activated delayed fluorescence emitter by introducing intramolecular hydrogen bond, *Chem. Eng. J.*, 2022, **448**, 137717.
14 Z. Cai, X. Wu, H. Liu, J. Guo, D. Yang, D. Ma, Z. Zhao and B. Z. Tang, Realizing Record-High Electroluminescence Efficiency of 31.5% for Red Thermally Activated Delayed Fluorescence Molecules, *Angew. Chem., Int. Ed.*, 2021, **60**, 23635–23640.
15 J.-L. He, F.-C. Kong, B. Sun, X.-J. Wang, Q.-S. Tian, J. Fan and L.-S. Liao, Highly efficient deep-red TADF organic light-emitting diodes via increasing the acceptor strength of fused polycyclic aromatics, *Chem. Eng. J.*, 2021, **424**, 130470.
16 J.-X. Chen, Y.-F. Xiao, K. Wang, D. Sun, X.-C. Fan, X. Zhang, M. Zhang, Y.-Z. Shi, J. Yu, F.-X. Geng, C.-S. Lee and X.-H. Zhang, Managing Locally Excited and Charge-Transfer Triplet States to Facilitate Up-Conversion in Red TADF Emitters That Are Available for Both Vacuum- and Solution-Processes, *Angew. Chem., Int. Ed.*, 2021, **60**, 2478–2484.
17 T. Hatakeyama, K. Shiren, K. Nakajima, S. Nomura, S. Nakatsuka, K. Kinoshita, J. Ni, Y. Ono and T. Ikuta, Ultrapure Blue Thermally Activated Delayed Fluorescence Molecules: Efficient HOMO–LUMO Separation by the Multiple Resonance Effect, *Adv. Mater.*, 2016, **28**, 2777–2781.
18 Y. Zhang, D. Zhang, J. Wei, Z. Liu, Y. Lu and L. Duan, Multi-Resonance Induced Thermally Activated Delayed Fluorophores for Narrowband Green OLEDs, *Angew. Chem., Int. Ed.*, 2019, **58**, 16912–16917.
19 Y. C. L. Xu, C. L. Li, Z. Q. Wang, J. X. Xue, J. N. Wang, Q. Y. Cai and X. L. Wang, Y, Highly Efficient

Electroluminescent Materials with High Color Purity Based on Strong Acceptor Attachment onto B-N-Containing Multiple Resonance Frameworks, *CCS Chem*, 2021, **3**, 2077–2091.

20 X. Wu, J.-W. Huang, B.-K. Su, S. Wang, L. Yuan, W.-Q. Zheng, H. Zhang, Y.-X. Zheng, W. Zhu and P.-T. Chou, Fabrication of Circularly Polarized MR-TADF Emitters with Asymmetrical Peripheral-Lock Enhancing Helical B/N-Doped Nanographenes, *Adv. Mater.*, 2022, **34**, 2105080.

21 M. Yang, S. Shikita, H. Min, I. S. Park, H. Shibata, N. Amanokura and T. Yasuda, Wide-Range Color Tuning of Narrowband Emission in Multi-resonance Organoboron Delayed Fluorescence Materials through Rational Imine/Amine Functionalization, *Angew. Chem., Int. Ed.*, 2021, **60**, 23142–23147.

22 Y. Qi, W. Ning, Y. Zou, X. Cao, S. Gong and C. Yang, Peripheral Decoration of Multi-Resonance Molecules as a Versatile Approach for Simultaneous Long-Wavelength and Narrowband Emission, *Adv. Funct. Mater.*, 2021, **31**, 2102017.

23 Y. Zhang, D. Zhang, T. Huang, A. J. Gillett, Y. Liu, D. Hu, L. Cui, Z. Bin, G. Li, J. Wei and L. Duan, Multi-Resonance Deep-Red Emitters with Shallow Potential-Energy Surfaces to Surpass Energy-Gap Law, *Angew. Chem., Int. Ed.*, 2021, **60**, 20498–20503.

24 Y. Liu, C. Li, Z. Ren, S. Yan and M. R. Bryce, All-organic thermally activated delayed fluorescence materials for organic light-emitting diodes, *Nat. Rev. Mater.*, 2018, **3**, 18020.

25 W. Yang, W. Ning, H. Jungchi, T. Liu, X. Yin, C. Ye, S. Gong and C. Yang, Polycyclic phenazine-derived rigid donors construct thermally activated delayed fluorescence emitters for highly efficient orange OLEDs with extremely low roll-off, *Chem. Eng. J.*, 2022, **438**, 135571.

26 Y. Xu, Z. Cheng, Z. Li, B. Liang, J. Wang, J. Wei, Z. Zhang and Y. Wang, Molecular-Structure and Device-Configuration Optimizations toward Highly Efficient Green Electroluminescence with Narrowband Emission and High Color Purity, *Adv. Optical Mater.*, 2020, **8**, 1902142.

27 Y. Xu, C. Li, Z. Li, Q. Wang, X. Cai, J. Wei and Y. Wang, Constructing Charge-Transfer Excited States Based on Frontier Molecular Orbital Engineering: Narrowband Green Electroluminescence with High Color Purity and Efficiency, *Angew. Chem., Int. Ed.*, 2020, **59**, 17442–17446.

28 J. Bian, S. Chen, L. Qiu, R. Tian, Y. Man, Y. Wang, S. Chen, J. Zhang, C. Duan, C. Han and H. Xu, Ambipolar Self-Host Functionalization Accelerates Blue Multi-Resonance Thermally Activated Delayed Fluorescence with Internal Quantum Efficiency of 100%, *Adv. Mater.*, 2022, **34**, 2110547.

29 J.-W. Huang, Y.-C. Hsu, X. Wu, S. Wang, X.-Q. Gan, W.-Q. Zheng, H. Zhang, Y.-Z. Gong, W.-Y. Hung, P.-T. Chou and W. Zhu, Influence of charge transfer strength on emission bandwidth for multiple-resonance emitters via systematically tuning the acceptor–donor assembly, *J. Mater. Chem. C*, 2022, **10**, 7866–7874.

30 T. Hua, Y.-C. Liu, C.-W. Huang, N. Li, C. Zhou, Z. Huang, X. Cao, C.-C. Wu and C. Yang, High-efficiency and low roll-off deep-blue OLEDs enabled by thermally activated delayed fluorescence emitter with preferred horizontal dipole orientation, *Chem. Eng. J.*, 2022, **433**, 133598.

31 X. Cai, J. Xue, C. Li, B. Liang, A. Ying, Y. Tan, S. Gong and Y. Wang, Achieving 37.1% Green Electroluminescent Efficiency and 0.09 eV Full Width at Half Maximum Based on a Ternary Boron-Oxygen-Nitrogen Embedded Polycyclic Aromatic System, *Angew. Chem., Int. Ed.*, 2022, **61**, e202200337.

32 Q. Zhang, B. Li, S. Huang, H. Nomura, H. Tanaka and C. Adachi, Efficient blue organic light-emitting diodes employing thermally activated delayed fluorescence, *Nat. Photonics*, 2014, **8**, 326–332.

33 D. H. Ahn, S. W. Kim, H. Lee, I. J. Ko, D. Karthik, J. Y. Lee and J. H. Kwon, Highly efficient blue thermally activated delayed fluorescence emitters based on symmetrical and rigid oxygen-bridged boron acceptors, *Nat. Photonics*, 2019, **13**, 540–546.

34 T. Chen, C.-H. Lu, C.-W. Huang, X. Zeng, J. Gao, Z. Chen, Y. Xiang, W. Zeng, Z. Huang, S. Gong, C.-C. Wu and C. Yang, Tuning the emissive characteristics of TADF emitters by fusing heterocycles with acridine as donors: highly efficient orange to red organic light-emitting diodes with EQE over 20%, *J. Mater. Chem. C*, 2019, **7**, 9087–9094.

35 J. Liang, C. Li, Y. Cui, Z. Li, J. Wang and Y. Wang, Rational design of efficient orange-red to red thermally activated delayed fluorescence emitters for OLEDs with external quantum efficiency of up to 26.0% and reduced efficiency roll-off, *J. Mater. Chem. C*, 2020, **8**, 1614–1622.

36 H. Liu, J. Li, W.-C. Chen, X. Lv, C. Zhou, C.-S. Lee and C. Yang, Efficient Yellow Thermally Activated Delayed Fluorescent Emitters Based on 3,5-Dicyanopyridine Acceptors, *J. Phys. Chem. C*, 2020, **124**, 25489–25498.

37 F.-M. Xie, P. Wu, S.-J. Zou, Y.-Q. Li, T. Cheng, M. Xie, J.-X. Tang and X. Zhao, Efficient Orange–Red Delayed Fluorescence Organic Light-Emitting Diodes with External Quantum Efficiency over 26%, *Adv. Electron. Mater.*, 2020, **6**, 1900843.

38 D. Karthik, Y. H. Jung, H. Lee, S. Hwang, B.-M. Seo, J.-Y. Kim, C. W. Han and J. H. Kwon, Acceptor–Donor–Acceptor-Type Orange–Red Thermally Activated Delayed Fluorescence Materials Realizing External Quantum Efficiency Over 30% with Low Efficiency Roll-Off, *Adv. Mater.*, 2021, **33**, 2007724.

39 S. Wang, Z. Cheng, X. Song, X. Yan, K. Ye, Y. Liu, G. Yang and Y. Wang, Highly Efficient Long-Wavelength Thermally Activated Delayed Fluorescence OLEDs Based on Dicyanopyrazino Phenanthrene Derivatives, *ACS Appl. Mater. Interfaces*, 2017, **9**, 9892–9901.

40 W. Zeng, H.-Y. Lai, W.-K. Lee, M. Jiao, Y.-J. Shiu, C. Zhong, S. Gong, T. Zhou, G. Xie, M. Sarma, K.-T. Wong, C.-C. Wu and C. Yang, Achieving Nearly 30% External Quantum Efficiency for Orange–Red Organic Light Emitting Diodes by Employing Thermally Activated Delayed Fluorescence Emitters Composed of 1,8-Naphthalimide-Acridine Hybrids, *Adv. Mater.*, 2018, **30**, 1704961.

41 S. Kothavale, W. J. Chung and J. Y. Lee, Rational Molecular Design of Highly Efficient Yellow-Red Thermally Activated

Delayed Fluorescent Emitters: A Combined Effect of Auxiliary Fluorine and Rigidified Acceptor Unit, *ACS Appl. Mater. Interfaces*, 2020, **12**, 18730–18738.

42 H. Wang, B. Zhao, P. Ma, Z. Li, X. Wang, C. Zhao, X. Fan, L. Tao, C. Duan, J. Zhang, C. Han, G. Chen and H. Xu, A red thermally activated delayed fluorescence emitter employing dipyridophenazine with a gradient multi-inductive effect to improve radiation efficiency, *J. Mater. Chem. C*, 2019, **7**, 7525–7530.

43 Y.-Y. Wang, Y.-L. Zhang, K. Tong, L. Ding, J. Fan and L.-S. Liao, Highly efficient red thermally activated delayed fluorescence materials based on a cyano-containing planar acceptor, *J. Mater. Chem. C*, 2019, **7**, 15301–15307.

44 J. Fan, J. Miao, N. Li, Y. Zeng, C. Ye, X. Yin and C. Yang, A dual rigid donor and acceptor enabling red thermally activated delayed fluorescence emitters for efficient OLEDs with low efficiency roll-off, *J. Mater. Chem. C*, 2022, **10**, 10255–10261.

45 K. R. Naveen, S. J. Hwang, H. Lee and J. H. Kwon, Narrow Band Red Emission Fluorophore with Reasonable Multiple Resonance Effect, *Adv. Electron. Mater.*, 2022, **8**, 2101114.

46 F.-M. Xie, H.-Z. Li, G.-L. Dai, Y.-Q. Li, T. Cheng, M. Xie, J.-X. Tang and X. Zhao, Rational Molecular Design of Dibenzo[a,c]phenazine-Based Thermally Activated Delayed Fluorescence Emitters for Orange-Red OLEDs with EQE up to 22.0%, *ACS Appl. Mater. Interfaces*, 2019, **11**, 26144–26151.

47 X. Gong, P. Li, Y.-H. Huang, C.-Y. Wang, C.-H. Lu, W.-K. Lee, C. Zhong, Z. Chen, W. Ning, C.-C. Wu, S. Gong and C. Yang, A Red Thermally Activated Delayed Fluorescence Emitter Simultaneously Having High Photoluminescence Quantum Efficiency and Preferentially Horizontal Emitting Dipole Orientation, *Adv. Funct. Mater.*, 2020, **30**, 1908839.

48 J. Li, T. Nakagawa, J. MacDonald, Q. Zhang, H. Nomura, H. Miyazaki and C. Adachi, Highly Efficient Organic Light-Emitting Diode Based on a Hidden Thermally Activated Delayed Fluorescence Channel in a Heptazine Derivative, *Adv. Mater.*, 2013, **25**, 3319–3323.

49 Y. Zou, J. Hu, M. Yu, J. Miao, Z. Xie, Y. Qiu, X. Cao and C. Yang, High-Performance Narrowband Pure-Red OLEDs with External Quantum Efficiencies up to 36.1% and Ultra-low Efficiency Roll-Off, *Adv. Mater.*, 2022, **34**, 2201442.

50 P. Data, P. Pander, M. Okazaki, Y. Takeda, S. Minakata and A. P. Monkman, Dibenzo[a,j]phenazine-Cored Donor–Acceptor–Donor Compounds as Green-to-Red/NIR Thermally Activated Delayed Fluorescence Organic Light Emitters, *Angew. Chem., Int. Ed.*, 2016, **55**, 5739–5744.

51 J.-X. Chen, K. Wang, C.-J. Zheng, M. Zhang, Y.-Z. Shi, S.-L. Tao, H. Lin, W. Liu, W.-W. Tao, X.-M. Ou and X.-H. Zhang, Red Organic Light-Emitting Diode with External Quantum Efficiency beyond 20% Based on a Novel Thermally Activated Delayed Fluorescence Emitter, *Adv. Sci.*, 2018, **5**, 1800436.

52 Y.-Y. Wang, K.-N. Tong, K. Zhang, C.-H. Lu, X. Chen, J.-X. Liang, C.-K. Wang, C.-C. Wu, M.-K. Fung and J. Fan, Positive impact of chromophore flexibility on the efficiency of red thermally activated delayed fluorescence materials, *Mater. Horiz.*, 2021, **8**, 1297–1303.

53 A. Kumar, H. Y. Shin, T. Lee, J. Jung, B. J. Jung and M. H. Lee, Doubly Boron-Doped TADF Emitters Decorated with ortho-Donor Groups for Highly Efficient Green to Red OLEDs, *Chem. – Eur. J.*, 2020, **26**, 16793–16801.

54 M. Yang, I. S. Park and T. Yasuda, Full-Color, Narrowband, and High-Efficiency Electroluminescence from Boron and Carbazole Embedded Polycyclic Heteroaromatics, *J. Am. Chem. Soc.*, 2020, **142**, 19468–19472.

55 W. Zeng, T. Zhou, W. Ning, C. Zhong, J. He, S. Gong, G. Xie and C. Yang, Realizing 22.5% External Quantum Efficiency for Solution-Processed Thermally Activated Delayed-Fluorescence OLEDs with Red Emission at 622 nm via a Synergistic Strategy of Molecular Engineering and Host Selection, *Adv. Mater.*, 2019, **31**, 1901404.

56 J. Xue, Q. Liang, R. Wang, J. Hou, W. Li, Q. Peng, Z. Shuai and J. Qiao, Highly Efficient Thermally Activated Delayed Fluorescence via J-Aggregates with Strong Intermolecular Charge Transfer, *Adv. Mater.*, 2019, **31**, 1808242.

57 Y. Sun, W. Sun, W. Liu, X. Li, J. Yin and L. Zhou, Efficient Nondoped Pure Red/Near-Infrared TADF OLEDs by Designing and Adjusting Double Quantum Wells Structure, *ACS Appl. Electron Mater.*, 2022, **4**, 3615–3622.

58 C. Li, R. Duan, B. Liang, G. Han, S. Wang, K. Ye, Y. Liu, Y. Yi and Y. Wang, Deep-Red to Near-Infrared Thermally Activated Delayed Fluorescence in Organic Solid Films and Electroluminescent Devices, *Angew. Chem., Int. Ed.*, 2017, **56**, 11525–11529.

59 Y.-L. Zhang, Q. Ran, Q. Wang, Y. Liu, C. Hänisch, S. Reineke, J. Fan and L.-S. Liao, High-Efficiency Red Organic Light-Emitting Diodes with External Quantum Efficiency Close to 30% Based on a Novel Thermally Activated Delayed Fluorescence Emitter, *Adv. Mater.*, 2019, **31**, 1902368.